

EXAMPLE OF RESULTS FROM THE PROPOSED WG1/WG4 CASE ON THE DAYTIME CONVECTIVE DEVELOPMENT OVER LAND

Wojciech W. Grabowski

National Center for Atmospheric Research, Boulder, Colorado, USA, e-mail:
grabow@ncar.ucar.edu

Key words: convection, diurnal cycle

Abstract. *This document presents results from numerical simulations of an idealized case of daytime convective development over land. The case is based on observations collected in TRMM/LBA field project in Rondonia, Brazil. Results are presented from two different 3D simulations that start from the early morning sounding and are driven primarily by increasing surface fluxes. The first simulation uses a high spatial resolution and focuses on the formation and evolution of well-mixed cloud-topped boundary layer. The second simulation, which uses lower spatial resolution and larger computational domain, aims to resolve deep convection later in the day. The results illustrate various aspects of convective development over land and are used here to stimulate collaboration between boundary layer and deep convection working groups of the GCSS.*

1 Simulation details

The purpose of this case is to investigate the development of the daytime convective boundary layer over land and the transition from shallow to deep convection. The actual sounding and the evolution of surface fluxes as the day progresses come from observations on February 23, 1999, during the TRMM-LBA field campaign in Rondonia, Brazil. The challenging aspect of this case is the wide range of spatial scales involved. The case features the development of a well-mixed cloud-topped boundary layer from the early morning sounding, development of shallow convection as surface fluxes increase, and transition from shallow to deep convection. This case does not feature any "large-scale" forcing, i.e., no advective tendencies of temperature and moisture are specified as the simulation progresses. The input data are: i) initial sounding; ii) evolving surface temperature and moisture fluxes; and iii) evolving profiles of radiative cooling. The simulation can be performed in either 2D or 3D, with 2D models aligned in the E-W direction. The lateral boundary conditions are cyclic and flat (i.e., no topography) free-slip (i.e., no surface friction) lower boundary is assumed.

The results presented below were obtained using the massively parallel (Anderson et al. 1997) Eulerian version of the three-dimensional, two-time-level nonhydrostatic Eulerian/semi-Lagrangian (EULAG) anelastic fluid model of Smolarkiewicz and Margolin (1997). The model applies a simple warm rain and ice parameterization of Grabowski (1998) and uses a TKE approach to represent subgrid-scale transports.

In the shallow convection setup, the horizontal/vertical resolution is 50/25m using a grid of 128x128x161 in (x,y,z). The shallow convection simulation is run for 3 hrs as convection approaches the upper boundary of the domain (at 4 km) toward the end of the 3hr period. In the deep convection case, 500/125 m resolution in horizontal/vertical is used with the same number of gridpoints as in the shallow convection case (i.e., 128x128x161). The deep convection simulation is run for 6 hrs. To provide small-scale excitation, surface fluxes are not applied homogeneously across the domain, but they include a random component, with the amplitude equal to 10% of the flux value and random numbers generated every time step. Moreover, random perturbations of the temperature and water vapor, with the amplitude of 0.1K and 0.1g/kg for temperature and moisture, respectively, are also applied in the lowest 9 model levels every 15 minutes for both shallow convection and deep convection simulations.

2 Results to be presented

The following quantities are used in the comparison of model simulations:

- cloud fraction (defined as a fraction of the horizontal domain covered by cloudy columns; a column is considered cloudy if the total condensate mixing ratio at any level of the column is larger than 0.1 g/kg);
- height of the center of mass of the total condensate field (defined as $z_{cm} = \int Qz dV / \int Q dV$ where Q is the total condensate and the integration is over the entire computational

domain);

- temperature and moisture profiles in the lower troposphere;
- surface precipitation rate.

All but the last quantity are analyzed based on model results archived every 10 minutes of the simulation; surface precipitation is archived every model time step.

3 Boundary layer development: results from 3D shallow convection simulations

Figures 1 and 2 show evolutions of the temperature profiles every 0.5 hr of the shallow convection simulation. Figure 1 shows the profiles in the lowest 1.5 km to illustrate boundary layer development, whereas Fig. 2 shows the temperature profiles and the maximum extent of convection (at times corresponding to the profiles) in the entire 4 km depth of the computational domain. The vertical extent of convection is shown by vertical bars which stretch from the lowest cloud base to the highest cloud top in the entire computational domain (note that the subsequent temperature profiles are shifted in horizontal by 3K to better show the extent of convection). Figure 1 shows that temperature profiles above the boundary layer are insignificantly affected by convection despite the significant vertical development of convection toward the end of the simulation. As the deep convection simulation shows, computational domain warms significantly later in the simulation (hour 3 and beyond).

Figures 3 and 4 are analogous to 1 and 2, but for the water vapor mixing ratio profiles. Note that, unlike the temperature profiles, the moisture profiles above the boundary layer are significantly affected by convection.

Figure 5 shows temporal evolutions of the cloud fraction and the height of the center of mass of the condensate field. The figure shows that shallow clouds (with the center of mass only 200-300m above the ground and cloud cover smaller than 0.1) appear as early as 1 hr into the simulation. The cloud fraction does not change significantly for another hour and the center of mass of the cloud field raises steadily. The last hour of the simulation features deepening clouds and increase of the cloud fraction. These results are consistent with the cloud extent shown in Fig. 2 and 4.

As far as the surface precipitation is concerned, only small amount of precipitation reaches the ground at the very end of shallow convection simulation (the domain averaged precipitation rate at 3 hrs is 0.04 mm/hr). Thus, it appears that using a numerical model capable of simulating nonprecipitating convection only is reasonable for the shallow convection case. This is relevant if WG1 is interested in this case because their models often do not allow precipitation.

4 Transition from shallow to deep convection: results from 3D deep convection simulations

Figures 6 and 7, in the format similar to Figs. 1 and 2, show the evolution of temperature profiles for the deep convection simulation. Figure 6 shows the profiles in the lowest 1.5 km to illustrate the structure of the boundary layer, whereas Fig. 7 shows the temperature profiles and the maximum extent of convection (at times corresponding to the profiles) across the entire troposphere (note that, as in Fig. 2, the subsequent temperature profiles are shifted in horizontal by 3 K to better show the extent of convection). The lower-tropospheric temperature profiles show the impact of lower vertical resolution applied in the deep convection simulation. Horizontal resolution has likely some impact on the boundary layer as well. Note that the model subgrid-scale TKE scheme does a rather poor job in representing well-mixed boundary layer. It would be interesting to see if models with more sophisticated boundary layer and/or turbulence parameterization can improve the boundary layer structure in the deep convection setup. Note that the vertical resolution applied in this case (125m) can still be considered relatively high when compared to traditional large-scale and climate models. The free-tropospheric temperatures show significant warming starting at 3 hours of the simulation; this is related to the domain-wide subsidence as a result of deep convection development..

Figures 8 and 9 show the profiles of the water vapor in the deep convection setup and are analogous to 3 and 4 for the shallow case. As in the temperature profiles, the impact of the low spatial resolution on the boundary layer is apparent.

Figure 10 shows temporal evolution of the cloud fraction and the height of the center of mass of the condensate field for the deep convection simulation. This figure should be compared to Fig. 5 for the shallow convection simulation. As the two figures show, clouds tend to develop later in the deep convection case and their vertical development is very rapid (e.g., the center of mass is only at about 1km in shallow convection simulation, but it is already at 3-4 km in the deep convection case). However, the depth of the computational domain applied in the shallow convection case is likely to small in the last hour of the simulation.

The evolution of the domain-averaged surface precipitation in the deep convection case shown in Fig. 11. Surface precipitation rapidly increases during third hour of the simulation and stabilizes at the rate of about 0.5 mm/hr. In the shallow convection case, there is only a trace of surface precipitation at the end of the simulation (not shown).

5 Summary

The purpose of this writeup is to present results from a particular model simulations of an idealized daytime convective development over land. Because convection is driven by the strong diurnal cycle of surface fluxes, capturing both the convective boundary layer development and transition from shallow to deep convection in a single simulation is difficult. The results presented herein are to motivate collaboration among relevant

Working Groups of GCSS to further our understanding of this problem and improve its representation in large-scale and climate models.

REFERENCES

- [1] W. W. Grabowski, "Toward cloud resolving modeling of large-scale tropical circulations: A simple cloud microphysics parameterization", *J. Atmos. Sci.*, **55**, 3283-3298 (1998).
- [2] W.D. Anderson, V. Grubišić, and P.K. Smolarkiewicz, "Performance of a massively parallel 3D non-hydrostatic atmospheric fluid model". *Proc. Int. Conf. on Parallel and Distributed Processing Techniques and Applications PDPTA '97*, Computer Science Research, Education, and Application Tech (CSREA), 645-651 (1997).
- [3] P.K. Smolarkiewicz, and L.G. Margolin, "On forward-in-time differencing for fluids: An Eulerian/semi-Lagrangian nonhydrostatic model for stratified flows", *Atmos. Ocean Special*, **35**, 127-152 (1997).

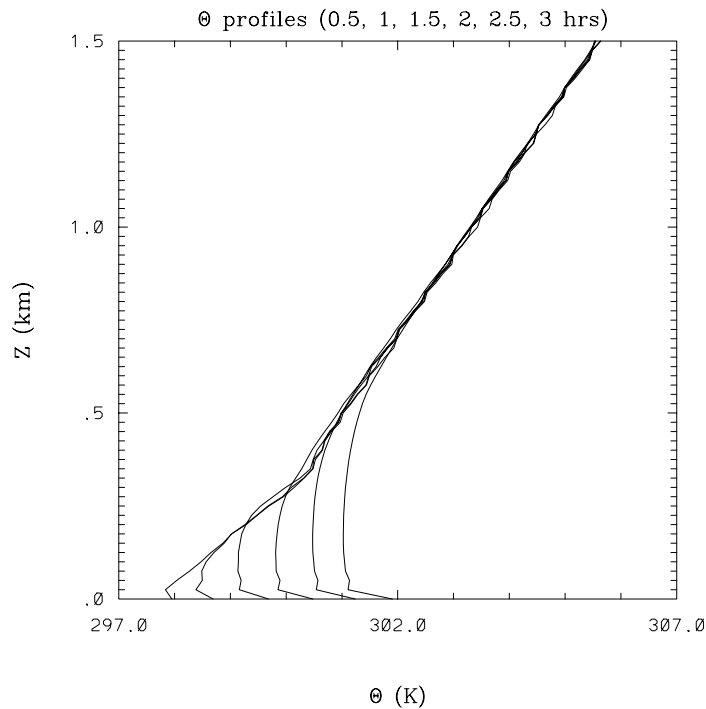


Figure 1: Potential temperature profiles in the lowest 1.5 km of the computational domain plotted every 0.5 hr of the simulation using high spatial resolution to capture boundary layer development (the shallow convection simulation).

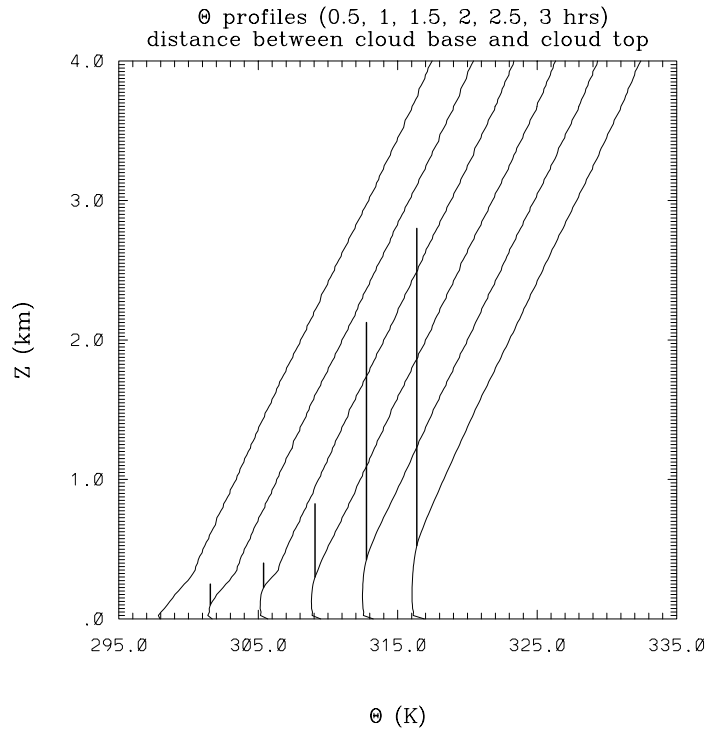


Figure 2: As Fig. 1, but for the entire depth of the computational domain. Vertical lines, connected to the profiles at the cloud-base temperature, show the vertical extent of clouds. Note that the temperature scale applies only for the profile at 0.5 hr; later profiles are shifted to the right for a better display.

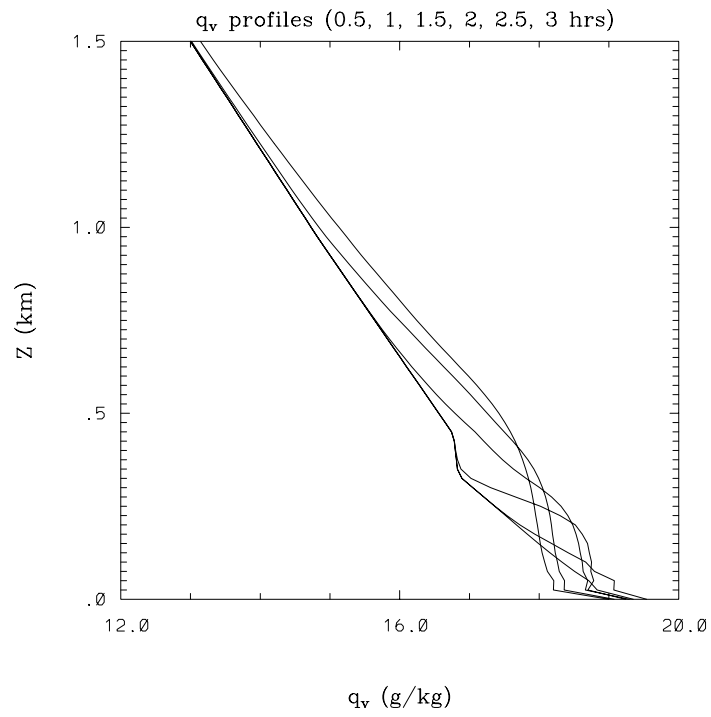


Figure 3: As Fig. 1, but for water vapor mixing ratio.

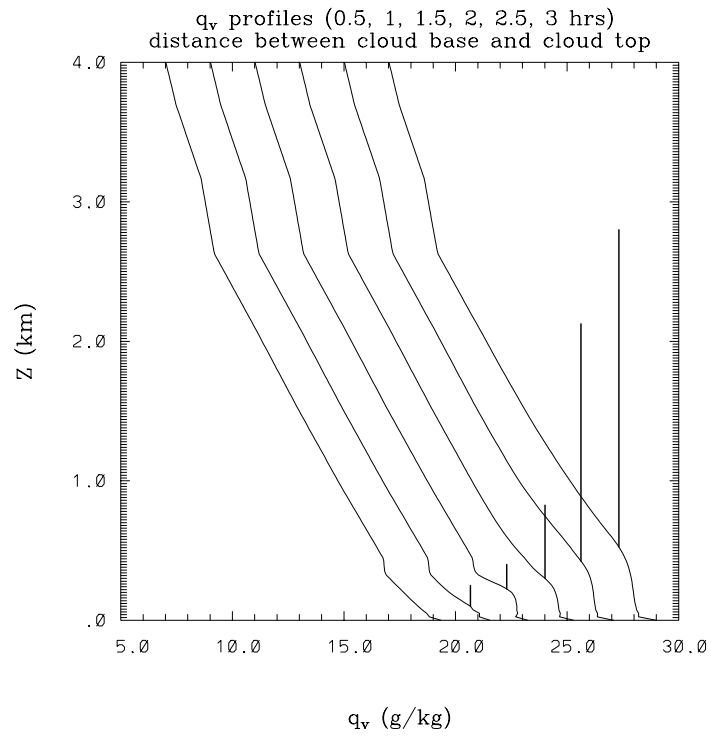


Figure 4: As Fig. 2, but for water vapor mixing ratio.

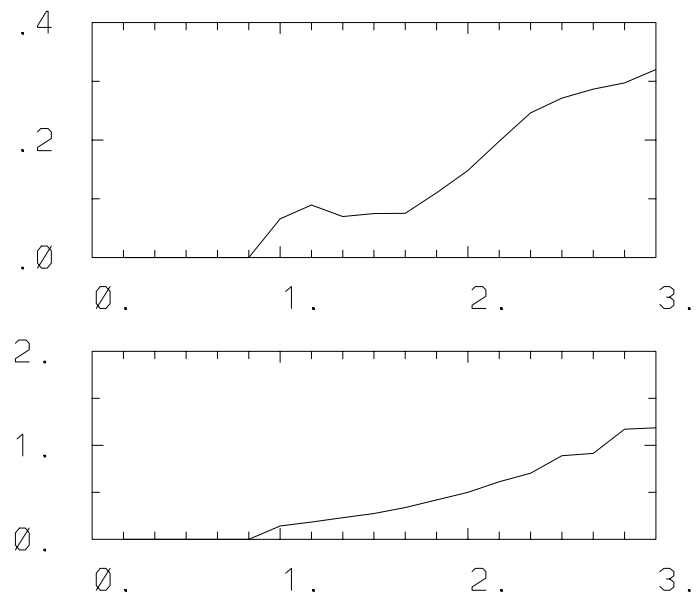


Figure 5: Evolution of the cloud fraction (upper panel) and height (in km) of the center of mass of the total condensate field (lower panel) for the shallow convection simulation.

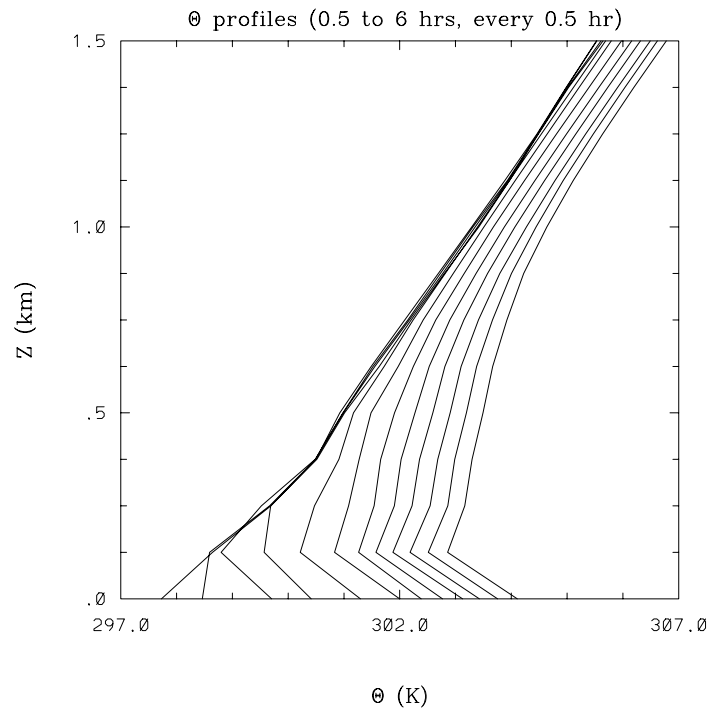


Figure 6: As Fig. 1, but for the simulation with deep computational domain and lower vertical resolution (deep convection setup). Note that this simulations is run for 6 hrs.

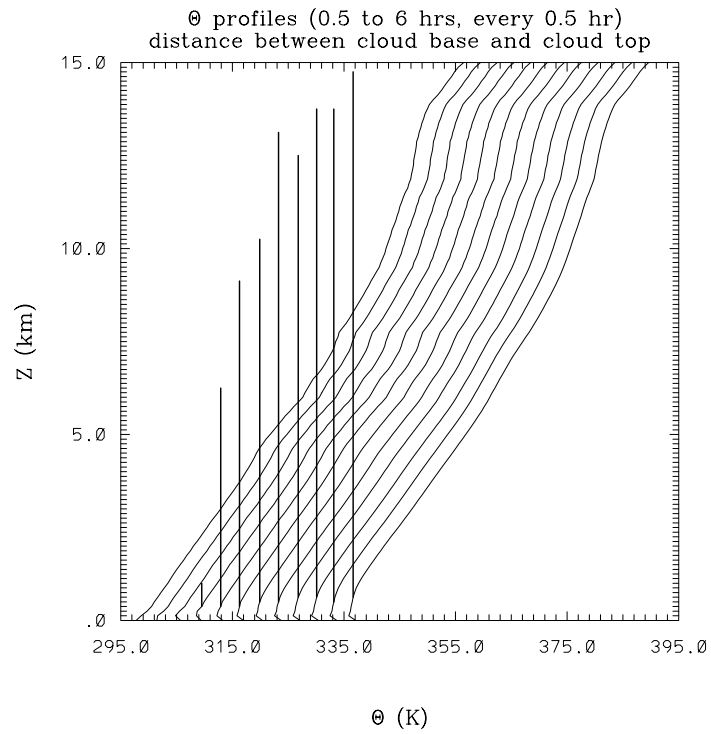


Figure 7: As Fig. 6, but for the 15-km depth of the computational domain. Note that the temperature scale applies only for the profile at 0.5 hr; later profiles are shifted to the right for a better display.

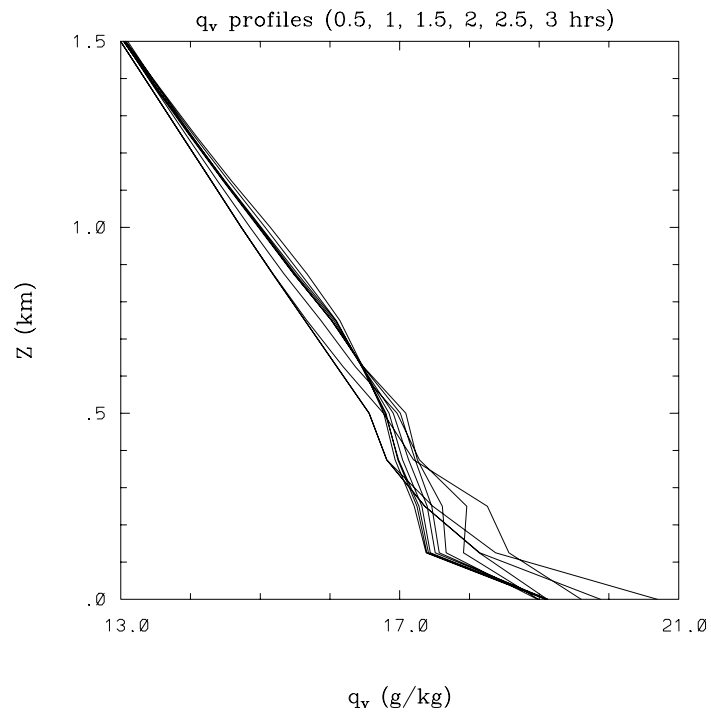


Figure 8: As Fig. 6, but for the profiles of the water vapor mixing ratio.

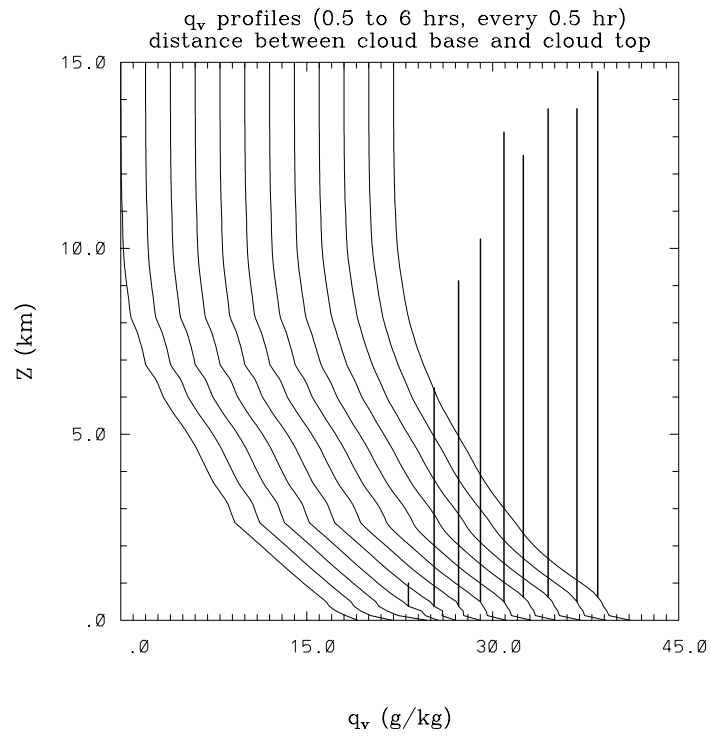


Figure 9: As Fig. 7, but for the profiles of the water vapor mixing ratio.

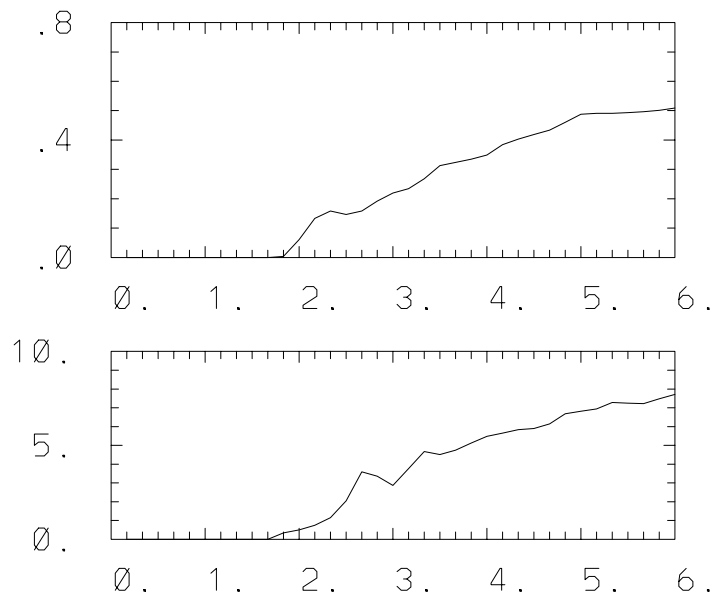


Figure 10: Evolution of the cloud fraction (upper panel) and height (in km) of the center of mass of the total condensate field (lower panel) for the deep convection simulation.

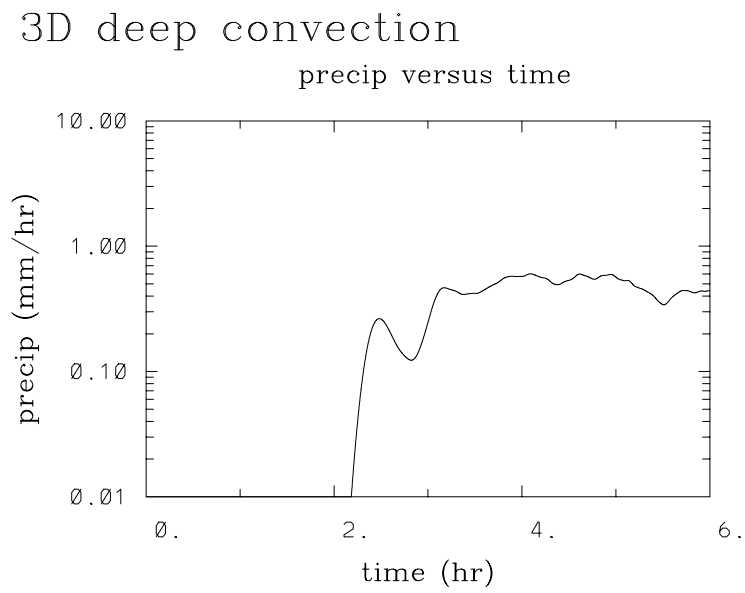


Figure 11: Evolution of the surface precipitation rate for the deep convection simulation.